Fabrication of the stainless steel surface with super durable one-direction superhydrophobicity and two-direction anisotropic wettability

Yanling Wan[1], Zhongxu Lian[1], Jinkai Xu[1], Zhankun Weng[2], Xiaoming Yin[1], Huadong Yu[1]

[1]*College of Mechanical and Electric Engineering, Changchun University of Science and Technology, Changchun 130022, People's Republic of China*
[2]*International Research Centre for Nano Handling and Manufacturing of China, Changchun University of Science and Technology, Changchun 130022, People's Republic of China*
E-mail: yuhuadong@cust.edu.cn

Published in Micro & Nano Letters; Received on 17th May 2014; Revised on 16th July 2014; Accepted on 18th August 2014

Inspired by the anisotropy of the rice leaf surface, high-speed wire electrical discharge machining (HS-WEDM) technology was used to build submillimetre-scale structures on the 304 stainless steel surfaces, and fluorination treatment was applied on the resulting surfaces. The wettability and microstructure of the resulting surfaces were investigated by a large depth 3D scanner, scanning electron microscopy and by the contact angle measuring instrument. The durability of the fabricated surface was evaluated by wear tests. Results show that the V-shaped groove arrays with a hierarchical structure on the processed surfaces are built by HS-WEDM. After the fluorination treatment, the as-machined surfaces show good one-direction superhydrophobicity and the obvious two-direction (the parallel and perpendicular groove directions) anisotropic wettability. The effect of the size of the V-shaped groove on the two-direction anisotropy is discussed. The wear tests show that the one-direction superhydrophobicity and the two-direction anisotropic sliding properties of the stainless steel surfaces are still exhibited after the tests. Fabricating rough surfaces by HS-WEDM is efficient and does not require complex process operation and large area three-dimensional features. This method can realise industrial production.

1. Introduction: In nature, the chemical composition and geometrical microstructure of the biological surface endows the surface with a certain wettability property while the transformation of the wettability property could give it unique features, such as the hydrophobicity of the lotus leaf covered by papillae accompanied by smaller protrusions of nanometre size [1], the anti-fogging function of the mastoid eye induced by the surface multiscale structures [2], water striders that have non-wetting legs that allow them to walk on water freely [3] and water droplets that cannot roll off because of the combination of hierarchical structures on rose petals [4–6]. In recent years, the rice leaf surface with its unique anisotropic wettability is becoming a hot subject of study in the field of functional materials. Unlike the wettability of the lotus leaf, the rice leaf surface is covered with a groove structure, which induces water droplets to roll along the direction of the leaf [1]. Inspired by the rice leaf surface, surfaces with unique functions have potential applications in droplet-directional transportation, fluidic control and so on [7–11]. Researchers have developed some preparative technologies such as photolithography [12, 13], interference lithography [14–19], electrospinning [20], surface wrinkling [21], electrochemical etching [22] and curvature-assisted droplet oscillation [23]. However, most of these methods are subject to certain limitations, such as tedious fabrication and expensive equipment, and it seems that there is not one report discussing the mechanical stability of the artificial anisotropic wettability surface. Mechanical stability is a serious problem which restricts the use of functional materials. A majority of functional surfaces have structures that are subject to being destroyed and thus losing usability once they encounter relatively high friction [24], which could be a defect in use. Therefore, preparing mechanically durable surfaces can make functional materials which can be useful in many circumstances.

In this Letter, a simple technology is demonstrated to fabricate the V-shaped groove arrays on the 304 stainless steel surfaces by high-speed wire electrical discharge machining (HS-WEDM), and craters have appeared both on the electrode and the workpiece surfaces. This is potentially useful to create roughness for good hydrophobic surfaces. In addition, there are several advantages of HS-WEDM. First, the controlled profile of the workpiece is obtained by a simple programming wire path [25]. Secondly, the hierarchical structure is created on the machined surfaces [26]. Here, the self-assembly technology was applied with low-surface-energy molecules of perfluorodecyltriethoxysilane on the resulting surfaces by HS-WEDM, and 304 stainless steel surfaces with good one-direction superhydrophobicity and obvious two-direction anisotropic wettability were successfully fabricated. The effect of the size of the V-shaped groove on two-direction anisotropic wettability were investigated. We also developed wear tests to evaluate the mechanical stability of the resulting surfaces with one-direction superhydrophobicity and two-direction anisotropic wettability. The potential industrial application values in microfluidic devices, liquid pumps and the evaporation-driven nanopatterns of the resulting surfaces are enlarged because of the properties of the one-direction superhydrophobicity and the two-direction anisotropic wettability remained after the strong wear tests, and such a sample fabrication method is expected to provide a new approaches for the mass industrial production of the surfaces.

2. Materials and methods

2.1. Materials: Polished 304 stainless steel of 2 cm thickness was used; it is better to choose a thinner material because of cutting efficiency and economic factors. In this work, the HS-WEDM could process the limit material size which is 70 mm × 500 mm × 500 mm; in other words, the sample preparation of the large area can be completed by HS-WEDM. Methanol (CH_3OH), perfluorodecyltriethoxysilane ($C_{16}H_{19}F_{17}O_3Si$), acetone (C_3H_6O) and alcohol (C_2H_6O) were also used. Distilled water was used for all experiments.

2.2. Experimental methods: HS-WEDM (DK7732) was used to build submillimetre-scale structures on the stainless steel surfaces, the structure model is as in Fig. 1. The specimens were fabricated

© The Institution of Engineering and Technology 2014

doi: 10.1049/mnl.2014.0275

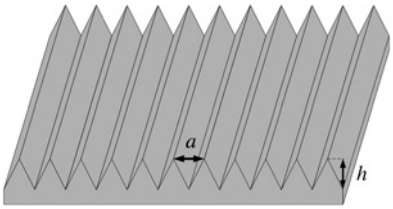


Figure 1 *Schematic diagram of processing structure*
a and *h* represent the width and depth of V-shaped groove arrays

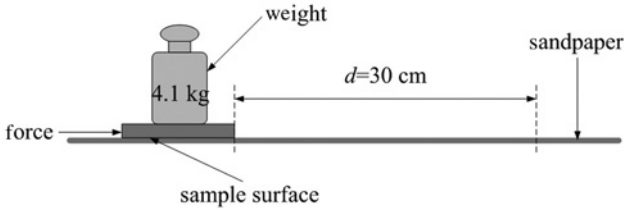


Figure 2 *Schematic diagram of wear test*

with a pulse width of 48 μs, pulse interval of 336 μs, wire speed of 50 Hz and four power tubes. After this, several steps needed to be taken for the machined specimens. First, the fabricated specimens were cleaned with acetone, ethano, and distilled water successively for about 15 min to remove the cutting fluid of the resulting surface. Secondly, the specimens were dried in a dying box at 80°C for about 20 min. Thirdly, the specimens were placed into a mass ratio of 1:100 mixed solutions made up of perfluorodecyltriethoxysilane and methanol for about 2 h. Finally, the specimens were placed in the drying box at a temperature of 135°C for about 1 h.

2.3. Characterisations: The surface morphology measurements were carried out on a VHX-1000 large depth 3D scanner and a JMS-6700FI scanning electron microscope (SEM), respectively. The water contact angle (WCA) was measured by an OCA20 optical contact angle measuring instrument. The droplet volume was 5 μl. The average WCA value was determined by measuring at five different positions of the same sample. The sliding contact angle was measured with 10 μl droplets by the tilting plate method as follows: first, the sample fixed onto the specimen stage was titled to a certain angle; secondly, one droplet of water was dripped onto the sample surface. If the water droplet rolls from the specimen's surface, the titled angle is the dynamic contact angle. If the water droplet does not roll, the specimen stage is titled to a certain angle of the water droplets rolling from the specimen stage.

Fig. 2 demonstrates how the linear abrasion device evaluates the durability of the sample. The specimen is loaded at about 40 kPa (in the area of the sample 10 cm^2, weight 4.1 kg), for each 30 cm slide in the wear test. After each wear test, the sample surface powder produced is blown off using a hair dryer, then the static contact angle and roll angle are measured. Sandpaper type: 240 mesh. The wear direction is perpendicular to the groove direction.

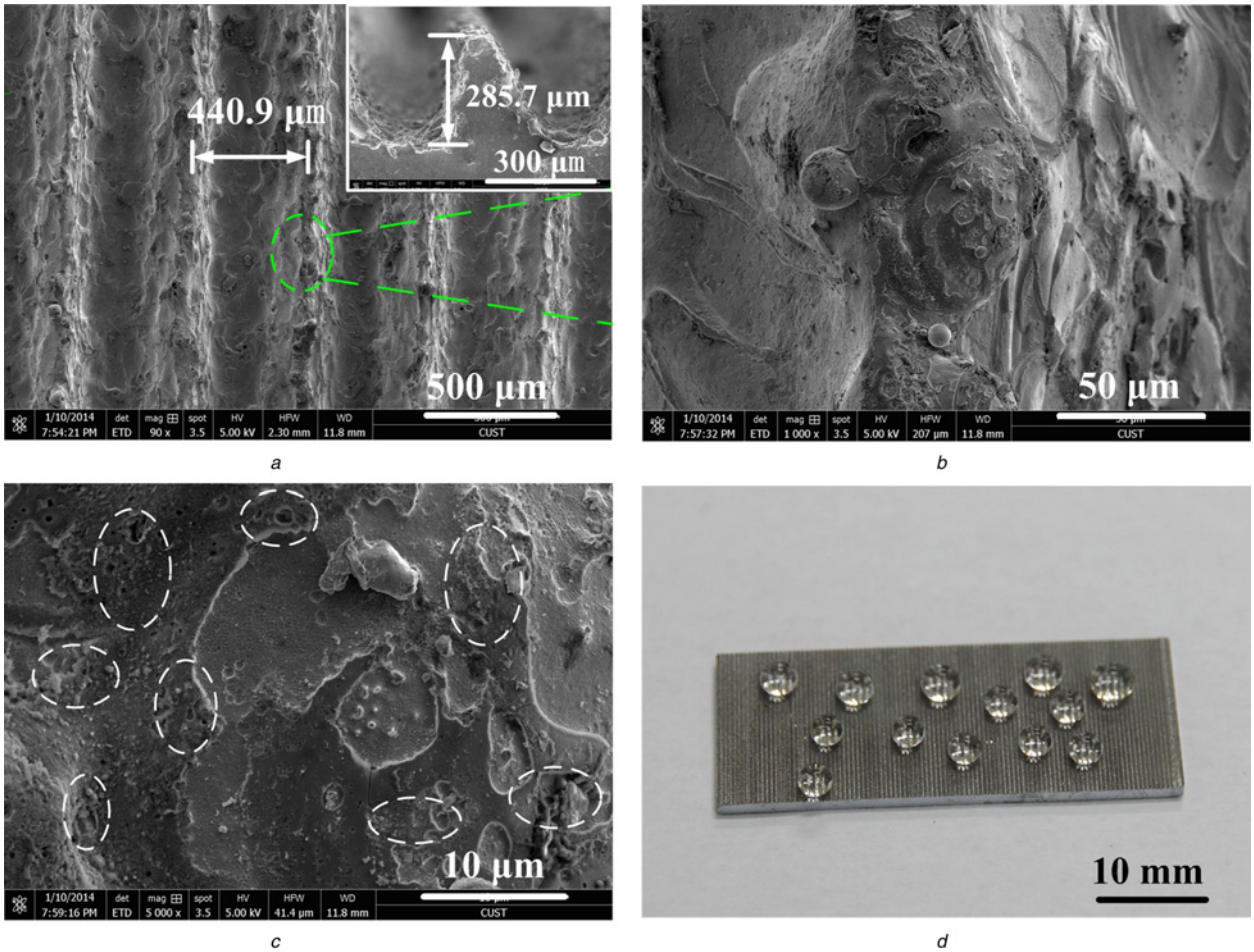


Figure 3 *SEM images of 304 stainless steel and the image of water droplet on the stainless steel surface*
a, *b*, and *c* SEM images of submillimetre-micro–nanoscale structure on the stainless steel surface
d Optical image of water droplet on the stainless steel surface

© The Institution of Engineering and Technology 2014

3. Results and discussion

3.1. Microstructure and hydrophobicity of the sample surface: Fig. 3*a* reveals the SEM images of the resulting surface. The surface was clearly uniformly covered by many submillimetre-scale V-shaped grooves, with an average depth of about 285.7 µm and width of 440.9 µm. That is, a hierarchical structure, containing submillimetre-micro–nanoscale structures, is formed on the stainless steel substrate, this being mainly attributed to the HS-WEDM spontaneously creating deposition points. Fig. 3*b* is an enlarged photograph of the microscale deposition point, the diameter of which is about 60 µm. In Fig. 3*c*, we can see that a large number of nanoscale pits appeared on the deposition point. In the HS-WEDM process for fabricating submillimetre-scale V-shaped grooves, the nanoscale pits were formed when sputtering the molten wire-electrode material on the stainless steel surface [27]. Fig. 3*d* is the optical image of a water droplet on the stainless steel surface with good one-direction superhydrophobicity (CA > 150°).

When using the OCA20 optical contact angle measuring instrument to measure the static contact angle and sliding angle on the sample's surfaces, it was found that water droplets exist in two-direction (the perpendicular and parallel groove directions) anisotropic wettability. For the sample without the low-surface-energy molecules, the contact angle measured in the direction perpendicular to the groove was 101.74° on the sample's surface; the contact angle in the direction parallel to the groove was 142.49°; and the water droplet was immersed into the groove. As is shown in Fig. 4, on the left, the static contact angle is extremely strong two-direction anisotropic, with a difference of 40.75°. However, for the sample with the low-surface-energy molecules, in Fig. 4 on the right side one can see that the water droplet stays at the top of the grooves. The static contact angle has been increased on the sample surface, the static contact angle in a direction perpendicular to the groove was 148° on the sample's surface and the static contact angle in the direction parallel to the groove was 154.36°, with a difference of 6.36°. Obviously, the stainless steel surface shows good one-direction superhydrophobicity, and the two-direction anisotropy of the contact angle decreases. When the water was dropped onto the sample's surface, the measured sliding angles were 10° and 5° along the perpendicular and parallel groove directions. Accordingly, building the submillimetre-scale V-shaped groove arrays may cause the two-direction anisotropic static contact angle of the water droplet on the stainless steel surface. The low-surface-energy molecules increase the hydrophobic properties of the sample's surface. Combining V-shaped groove arrays and low-surface-energy molecules, the water droplet located at the top of the grooves forms the solid–liquid–gas three-phase line with the sample surface. As a result, good one-direction superhydrophobicity in accordance with Cassie's state [28] is achieved.

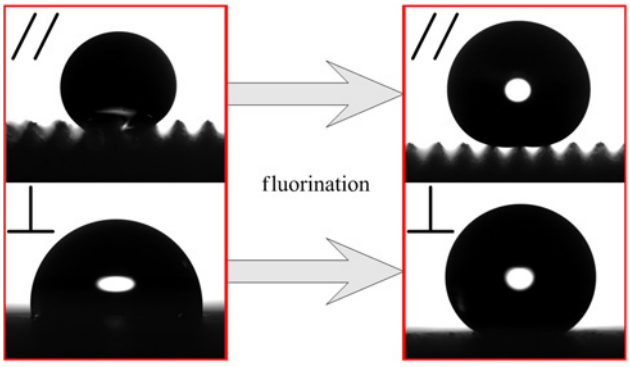


Figure 4 *Images of two-direction contact angle before and after fluorination treatment*

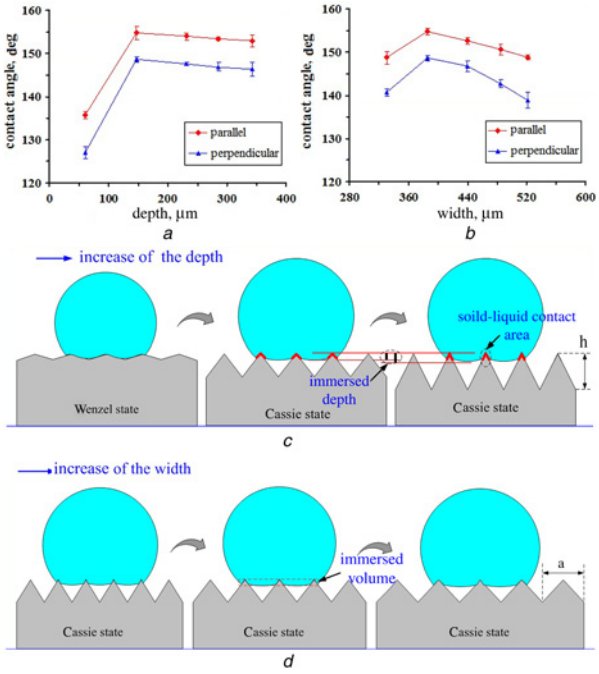


Figure 5 *Changes of the two-direction contact angles with the sizes of V-shaped groove on the fabricated stainless steel and their models*
a, *c* Increase of the depth and its model
b, *d* Increase of the width and its model

3.2. Sizes of the V-shaped groove affected the two-direction anisotropic wettability: Fig. 5 shows the changes in the static contact angles with the sizes of the V-shaped groove on the fabricated stainless steel by HS-WEDM. Fig. 5*a* shows that with the increase in groove depth (the width is 385.5 µm), the static contact angles of the sample's surface with the same width along the perpendicular and parallel groove directions increased. When it increases to a certain value, all the perpendicular and parallel contact angles decreased, but not many. It can be understood that water droplet and the surface contact state may be transformed

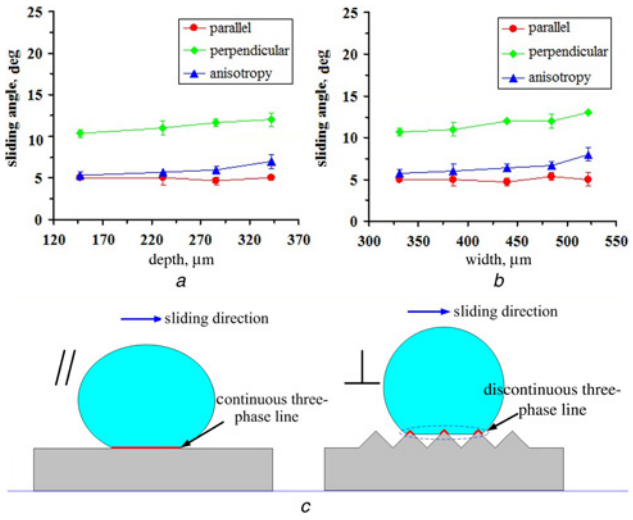


Figure 6 *Graph showing the two-direction sliding angles and anisotropy measured with the different sizes on the fabricated stainless steel surface and models of two sliding directions*
a, *b* Changes of the two-direction sliding angles and anisotropy with the depth and width of V-shaped groove
c Models of the continuous and discontinuous three-phase line of two sliding directions

© The Institution of Engineering and Technology 2014

doi: 10.1049/mnl.2014.0275

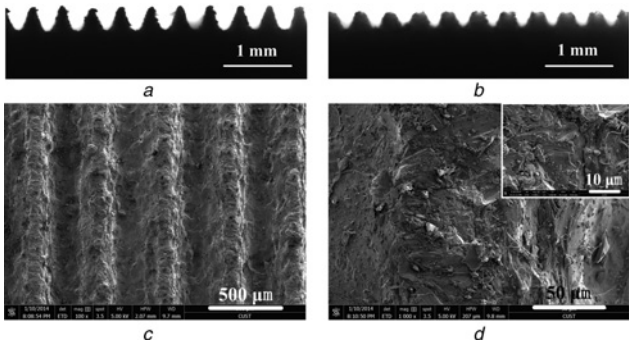


Figure 7 *Two-dimensional optical images and SEM images of the fabricated stainless steel surface before and after wear test*
a, *b* Two-dimensional optical images of the fabricated stainless steel surface before and after wear test
c, *d* SEM images after the wear test
Illustration within Fig. 7*d* is the SEM image of high magnification

from the 'Wenzel state' [29] into the 'Cassie state' [28] with the increase in depth. When the depth increased to a certain value, the water always remained located in two V-shaped grooves, and the width of the groove did not change, but the depth becomes large; this may lead the water droplet to drop into a deep place, so the contact angles of water droplets along the perpendicular and parallel groove directions decrease, the model is shown in Fig. 5*c*. In Fig. 5*b*, with the increase in groove width (the depth is 146.9 μm), the static contact angles along both the directions of the sample's surface increased, and then decreased. When the width of the V-shaped groove was 385.5 μm, the contact angle of the water droplet on the sample's surface reached the maximum value, being 154.78° for the droplets parallel to the grooves and 148.64° for the ones perpendicular to the grooves. Analysis shows that when the V-shaped groove width within the scope of 330.6–385.5 μm gradually increases, the numbers of the grooves in which the water droplet is located are from 3 to 2. In this case, the contact area of the solid–liquid interface may be reduced, and this may make the static contact angle increase. When the groove width reaches a critical value, the number of grooves in which the water droplet is located is still 2. However, because of the large width of the groove, the contact angle begins to decrease, and the model is as shown in Fig. 5*d*.

Fig. 6 shows the changes of the sliding angle and anisotropy with the sizes of the V-shaped groove. As is shown in Figs. 6*a* and *b*, there is no obvious variation of the parallel sliding angle along the direction of the grooves, which remains about 5°. The possible reason for this phenomenon is that when the water droplet is sliding on the parallel grooves, it does not have to overcome the large energy barrier as the solid–liquid–gas three-phase line is continuous. However, while the water droplet is sliding on the perpendicular grooves, the solid–liquid–gas three-phase line is discontinuous. Therefore, the perpendicular sliding angle depends on the depth and width of the V-shaped groove. With increase of the depth and the width, the volume of the water droplet into the groove gets bigger; therefore, it is necessary to provide a higher energy barrier to the slide. As a result, the water droplet sliding in the direction of the perpendicular groove enhances, and the model is as shown in Fig. 6*c*. From comparison with the two-direction anisotropic sliding, the trend of the anisotropic changes is consistent with the perpendicular sliding angle.

3.3. Mechanical stability: Generally, an artificial surface with high roughness is easily damaged under a big frictional force, which can lead to loss of performance. To extend the potential applicability of fabricated surfaces with anisotropic wettability, they have to exhibit high mechanical stability. In this study, the wear test was used to evaluate the mechanical stability of the fabricated surfaces with good one-direction superhydrophobicity and two-direction anisotropic wettability.

Fig. 7 shows the two-dimensional (2D) optical and SEM images of the 304 stainless steel surface before and after the wear test. Compared with the original sample, the top of the V-shaped grooves was seriously damaged after the sliding distance was 530 cm. The measured depth fell from 285.7 to 202.6 μm by the VHX-1000 large depth 3D scanner. In the SEM images, we can clearly see that there were a lot of micro–nanoscale scratches and some cracks at the top of the V-shaped grooves after the test; these cracks occurred because of the existence of fatigue wear in the wear mechanisms. Figs. 8*a* and *b* reveal the contact angle and sliding angle after the wear attempt, and there is no regularity change in the two-direction contact angle. The fabricated surface can withstand at least 530 cm of sliding distance without the good one-direction superhydrophobicity and the obvious two-direction anisotropic wettability. Greater sliding distance led to a decrease in the contact angle and the sliding angle. For example, when the sliding distance was 570 cm, the parallel contact angle and sliding angle was 146.52° and 10°, and the perpendicular contact angle and sliding angle was 142.95° and 14°, respectively. At this time, it is found that one-direction superhydrophobicity was lost, and the two-direction sliding angle values were >10°. A possible reason is that many micro–nanoscale scratches and some cracks appeared at the top of the V-shaped grooves with the increase of sliding distance, which could result in an uncertain contact area of the solid–liquid interface; the scratches and cracks are as shown in the illustration within Fig. 7*d*. The contact area of the solid–liquid interface may begin to enhance obviously when the sliding distance increases to reach a certain value, so the two-direction contact angle gradually becomes small.

The wear test showed that the fabricated surface still retained good one-direction superhydrophobicity and two-direction anisotropic wettability after the test. In addition, there is no obvious change in the two-direction contact angle and sliding angle after the samples (before and after the wear test) were placed in the air for four months.

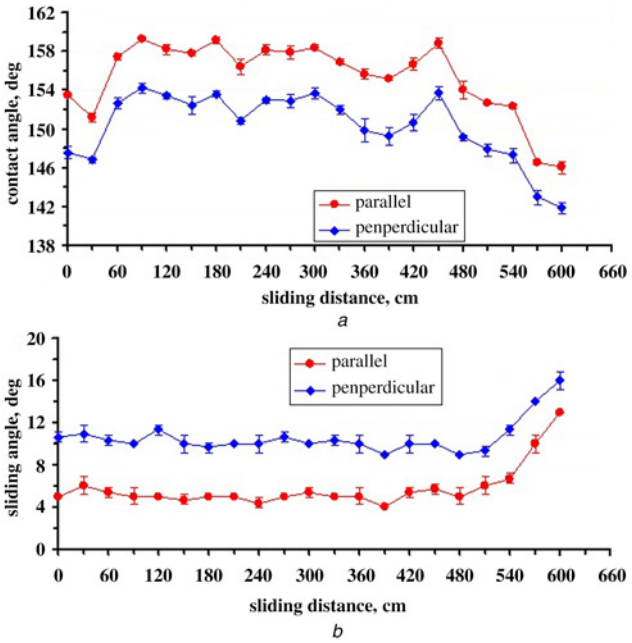


Figure 8 *Graph showing the contact angle and sliding angle measured with respect to wear attempts on a fabricated stainless steel surface*
a Contact angle
b Sliding angle

© The Institution of Engineering and Technology 2014

4. Conclusion: In this Letter, HS-WEDM technology has been demonstrated which is efficient, without complex process operation and large area 3D features to build V-shaped grooves on the 304 stainless steel surfaces. By combining with fluorination treatment, the 304 stainless steel surfaces with good one-direction superhydrophobicity and the obvious two-direction anisotropic wettability were successfully fabricated. Such a functional surface may be expected to have potential industrial applications for microfluidic devices, liquid pumps and evaporation-driven nanopatterns. The effect of the sizes of the V-shaped groove on two-direction anisotropic wettability is discussed, and the result may be useful for the design of controllable surfaces. Despite the micro–nanoscale scratches and some cracks that appeared during the process of wear at the top of the V-shaped grooves, the fabricated surface still retained good one-direction superhydrophobicity and two-direction anisotropic wettability at even high applied loads. Thus, this study is expected to provide a theoretical basis for the production of two-direction anisotropic engineering materials with supermechanical stability.

5. Acknowledgments: The authors acknowledge the support from the National Natural Science Foundation of China (NSFC, grant 51275056), the Jilin Province Science and Technology Development Program of China (grant 201201123) and the Changchun University of Science and Technology Young Scientists Foundation of China (grant 202000490).

6 References

[1] Feng L., Li S., Li Y., *ET AL.*: 'Super-hydrophobic surfaces: from natural to artificial', *Adv. Mater.*, 2002, **14**, (24), pp. 1857–1860
[2] Gao X., Yan X., Yao X., *ET AL.*: 'The dry-style antifogging properties of mosquito compound eyes and artificial analogues prepared by soft lithography', *Adv. Mater.*, 2007, **19**, (17), pp. 2213–2217
[3] Gao X.F., Jiang L.: 'Water-repellent legs of water striders', *Nature*, 2004, **432**, (7013), pp. 0028–0836
[4] Feng L., Zhang Y.N., Xi J.M., *ET AL.*: 'Petal effect: a superhydrophobic state with high adhesive force', *Langmuir*, 2008, **24**, (8), pp. 4114–4119
[5] Feng L., Zhang Y.A., Li M.Z., *ET AL.*: 'The structural color of red rose petals and their duplicates', *Langmuir*, 2010, **26**, (18), pp. 14885–14888
[6] Bhushan B., Her E.K.: 'Fabrication of superhydrophobic surfaces with high and low adhesion inspired from rose petal', *Langmuir*, 2010, **26**, (11), pp. 8207–8217
[7] Gau H.: 'Liquid morphologies on structured surfaces: from microchannels to microchips', *Science*, 1999, **283**, (5398), pp. 46–49
[8] Xu Q.F., Wang J.N., Smith I.H., *ET AL.*: 'Directing the transportation of a water droplet on a patterned superhydrophobic surface', *Appl. Phys. Lett.*, 2008, **93**, (23), pp. 233112
[9] Zhao B., Moore J.S., Beebe D.J.: 'Surface-directed liquid flow inside microchannels', *Science*, 2001, **291**, (5506), pp. 1023–1026
[10] Higgins A.M., Jones R.A.L.: 'Anisotropic spinodal dewetting as a route to self-assembly of patterned surfaces', *Nature*, 2000, **404**, (6777), pp. 476–478
[11] Ralf S., Martin B., Edward J.K., *ET AL.*: 'Wetting morphologies at microstructured surfaces', *Proc. Natl Acad. Sci. USA*, 2005, **102**, (6), pp. 1848–1852
[12] Morita M., Koga T., Otsuka H., *ET AL.*: 'Macroscopic-wetting anisotropy on the line-patterned surface of fluoroalkylsilane monolayers', *Langmuir*, 2005, **21**, (3), pp. 911–918
[13] Sommers A.D., Jacobi A.M.: 'Creating micro-scale surface topology to achieve anisotropic wettability on an aluminum surface', *J. Micromech. Microeng.*, 2006, **16**, (8), pp. 1571–1578
[14] Zhao Y., Lu Q.H., Li M., *ET AL.*: 'Anisotropic wetting characteristics on submicrometer-scale periodic grooved surface', *Langmuir*, 2007, **23**, (11), pp. 6212–6217
[15] Wu D., Chen Q.D., Yao J., *ET AL.*: 'A simple strategy to realize biomimetic surfaces with controlled anisotropic wetting', *Appl. Phys. Lett.*, 2010, **96**, (5), p. 053704
[16] Wu S.Z., Wu D., Yao J., *ET AL.*: 'One-step preparation of regular micropearl arrays for two-direction controllable anisotropic wetting', *Langmuir*, 2010, **26**, (14), pp. 12012–12016
[17] Wu S.Z., Wang J.N., Niu L.G., *ET AL.*: 'Reversible switching between isotropic and anisotropic wetting by one-direction curvature tuning on flexible superhydrophobic surfaces', *Appl. Phys. Lett.*, 2011, **98**, (8), pp. 81902–81904
[18] Xia D., Brueck S.R.: 'Strongly anisotropic wetting on one-dimensional nanopatterned surfaces', *Nano Lett.*, 2008, **8**, (9), pp. 2819–2824
[19] Xia D.Y., He X., Jiang Y.B., *ET AL.*: 'Tailoring anisotropic wetting properties on submicrometer-scale periodic grooved surfaces', *Langmuir*, 2010, **26**, (4), pp. 2700–2706
[20] Wu H., Zhang R., Sun Y., *ET AL.*: 'Biomimetic nanofiber patterns with controlled wettability', *Soft Mat.*, 2008, **4**, pp. 2429–2433
[21] Zheng Y.M., Gao X.F., Jiang L.: 'Directional adhesion of superhydrophobic butterfly wings', *Soft Mat.*, 2007, **3**, (2), pp. 178–182
[22] Yang X.L., Song J.L., Xu W.J., *ET AL.*: 'Anisotropic sliding of multiple-level biomimetic rice-leaf surfaces on aluminium substrates', *Micro Nano Lett.*, 2013, **8**, (11), pp. 801–804
[23] Wu D., Wang J.N., Wu S.Z., *ET AL.*: 'Three-level biomimetic rice-leaf surfaces with controllable anisotropic sliding', *Adv. Funct. Mater.*, 2011, **21**, (15), pp. 2927–2932
[24] Verho T., Bower C., Andrew P., *ET AL.*: 'Mechanically durable superhydrophobic surfaces', *Adv. Mater.*, 2011, **23**, (5), pp. 673–678
[25] Ho K.H., Newman S.T.: 'State of the art electrical discharge machining (EDM)', *Int. J. Mach. Tools Manuf.*, 2003, **43**, (13), pp. 1287–1300
[26] Bae W.G., Song K.Y., Rahmawan Y., *ET AL.*: 'One-step process for superhydrophobic metallic surfaces by wire electrical discharge machining', *ACS Appl. Mater. Interfaces.*, 2012, **4**, (7), pp. 3685–3691
[27] Huang C.A., Shih C.L., Li K.C., *ET AL.*: 'The surface alloying behavior of martensitic stainless steel cut with wire electrical discharge machine', *Appl. Surf. Sci.*, 2006, **252**, pp. 2915–2926
[28] Cassie A.B.D., Baxter S.: 'Wettability of porous surfaces', *Trans. Faraday Soc.*, 1944, **40**, pp. 546–551
[29] Wenzel R.N.: 'Resistance of solid surfaces to wetting by water', *Ind. Eng. Chem.*, 1936, **28**, (8), pp. 988–994

© The Institution of Engineering and Technology 2014

doi: 10.1049/mnl.2014.0275